FIR FU

# *FIR Center Report*

**FIR FU-111**

**October 2011**

# Photoconductive emission and detection of terahertz pulsed radiation using semiconductors and semiconductor devices

**Masahiko Tani, Kohji Yamamoto, Elmer S. Estacio, Christopher T. Que, Hidekazu Nakajima, Masakazu Hibi, Fumiaki Miyamaru, Seizi Nishizawa, and Masanori Hangyo**

*Research Center for Development of Far-Infrared Region*
*University of Fukui*

*Bunkyo 3-9-1, Fukui 910-8507, Japan*

Tel 81 776 27 8657
Fax 81 776 27 8770

# Photoconductive emission and detection of terahertz pulsed radiation using semiconductors and semiconductor devices

Masahiko Tani[1], Kohji Yamamoto[1], Elmer S. Estacio[1], Christopher T. Que[1], Hidekazu Nakajima[1], Masakazu Hibi[1], Fumiaki Miyamaru[2], Seizi Nishizawa[3], and Masanori Hangyo[4]

[1] *Research Center for Development of Far-Infrared Region, University of Fukui, 3-9-1 Bunkyo, Fukui 910-8507, Japan*

*E-mail: tani@fir.u-fukui.ac.jp*

[2] *Department of Physics, Faculty of Science, Shinshu University, Asahi 3-1-1, Matsumoto, Nagano 390-8621, Japan*

[3] *Advanced Infrared Spectroscopy Co., Ltd., 3-17-16, Sennin, Hachioji, Tokyo 193-0835, Japan*

[4] *Institute of Laser Engineering, Osaka University, 2-6 Yamadaoka, Suita, Osaka 565-0871, Japan*

**Abstract**

Recent studies on the techniques and development of photoconductive (PC) semiconductor devices for efficient generation and detection of terahertz (THz) pulsed radiation are reported. Firstly, the optimization of PC antenna design is discussed. The PC detection of THz pulsed radiation using low-temperature grown GaAs with 1.55-μm wavelength probe is then described. Finally, the enhancement of THz radiation from InSb by using a coupling lens and magnetic field is investigated. These results reveal valuable insights on the design of an efficient, compact, and cost-effective THz time-domain spectroscopy system based on 1.55-μm fs laser sources.

*Keywords*: Terahertz, photoconductive antenna, low-temperature-grown GaAs, 1.55-μm femtosecond laser, InSb, lens coupling, magnetic field enhancement

## 1. Introduction

After the pioneering works by Lee [1,2], Auston [3,4] and Mourou [5], the technique of generating pulsed terahertz (THz) radiation using femtosecond (fs) laser pulses has been studied intensively and has since been utilized for spectroscopy and sensing applications. This THz time-domain spectroscopy (THz-TDS) technique [6] is unlike other conventional spectroscopic methods. The dispersion spectrum (frequency dependence of the refractive index) of a sample is determined unambiguously without resorting to Kramers-Kronig analysis or other complementary methods. The THz-TDS technique is also considered to be a powerful tool in sensing and imaging applications. This spectroscopic imaging method is non-destructive and is described as a "see-through technique" which enables the evaluation of subsurface materials, as well as enclosed or encapsulated objects. The THz tomographic imaging of medical tablets [7-8] for quality control and the THz spectroscopic imaging of masterpieces of paintings for maintenance or restoration purposes [9], are such examples. However, for THz technology to be more feasible for industrial applications, the efficiency and cost of current THz-TDS system designs need to be significantly improved. For these reasons, it is essential to develop more efficient photoconductive (PC) semiconductor devices used for the generation and detection of pulsed THz radiation. Moreover, in the interest of developing compact and cost-effective THz-TDS systems, these PC devices need to be usable for 1.55-μm fs fiber lasers. In this report, we describe our studies on the following: (i) optimization of PC antenna design, (ii) PC detection of THz pulsed radiation using low-temperature grown (LTG) GaAs with 1.55-μm probe, and (iii) enhancement of THz radiation from InSb with a coupling substrate lens and an externally applied magnetic field.

## 2. Basic principle of photoconductive antenna

The PC antenna [10-15] is one of the most commonly used devices for emission and detection of pulsed THz radiation. The characteristic structure of a Hertzian dipole PC antenna is illustrated in Fig. 1. The dimensions of the PC gap $G$ are typically 5-10 μm, with the antenna width $W$ and length $L$, usually measuring 10-20 μm and 30-50 μm, respectively [10]. The microstripline antenna is fabricated on a semiconductor substrate using photolithographic techniques. The PC gap is usually biased with a dc voltage in conjunction with fs laser illumination, when used as a THz emitter. After excitation of the PC gap, photo-excited carriers are accelerated under the bias field; creating an ultrashort current pulse which decays with a time constant determined by the carrier lifetime in the substrate. The transient current, J(t), generates ultrashort pulses of electro-magnetic radiation having frequencies in the THz regime. In the electric dipole approximation, the field amplitude of the radiation is proportional to the time derivative of the photocurrent, J(t), in the far field:

$$E_{THz} \propto \frac{\partial J(t)}{\partial t} . \qquad (1)$$

The time derivative of the transient current at its peak is proportional to the averaged photocurrent , $\bar{J}$ , divided by the duty ratio of the current pulse; which can be approximated with the ratio of the lifetime of the photo carriers, $\tau_c$, and the interval of the pump-laser pulses, $T_{int}$. Therefore,

$$E_{THz}^{peak} \propto \Delta J \equiv \bar{J} \times \frac{T_{\text{int}}}{\tau_c} = \bar{K} V_b \times \frac{T_{\text{int}}}{\tau_c} = \bar{\sigma} \frac{W\delta}{G} V_b \frac{T_{\text{int}}}{\tau_c} = e\mu\tau_c n_e \frac{W\delta}{G} V_b \frac{T_{\text{int}}}{\tau_c}$$

$$= e\mu\tau_c \frac{(1-R)}{h\nu} \frac{P_{in}}{GW\delta} \frac{W\delta}{G} V_b \frac{T_{\text{int}}}{\tau_c} = e\mu T_{\text{int}} \frac{(1-R)}{h\nu} \frac{P_{in}}{G} \frac{V_b}{G} = e\mu \frac{(1-R)}{h\nu} \frac{Q_{in}}{G} E_b . \qquad (2)$$

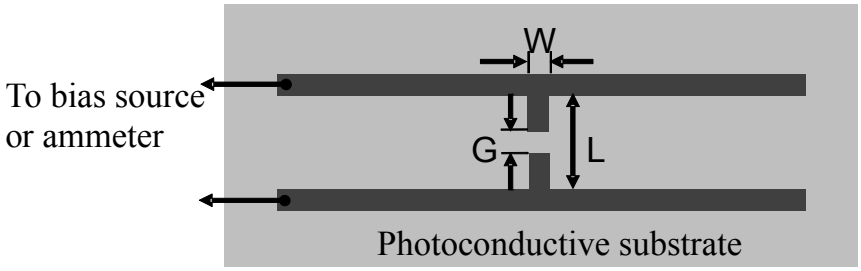


Fig. 1. Structure of a photoconductive dipole antenna.

Here, $\bar{K}$ is the time-averaged photo-conductance of the PC gap, $\bar{\sigma}$ , the time-averaged conductivity, δ, the absorption depth of the pump light, $n_e$, the photo-generated carrier density, $V_b$, the bias voltage, $E_b$ (=$V_b$/G), the bias field, μ, the mobility of the carriers, R, the reflectance of the PC substrate, hν, the photon energy of the pump laser, $P_{in}$, the averaged pump laser power, and $Q_{in}$ (=$T_{int}P_{in}$), the pulse energy of the pump laser. In the last expression of Eq.(2), the carrier lifetime, $\tau_c$, has disappeared because of the cancellation with the conductivity term ( $\bar{\sigma}$ =eμ$\tau_c n_e$). It should be noted, however, that a short carrier lifetime is also important for reducing the detector noise in a PC antenna, which originates from the thermal motion of the carriers.

From Eq.(2), the emission efficiency of a PC antenna is proportional to the carrier mobility but does not directly depend on carrier lifetime. Thus, a semiconductor material with high carrier mobility must be chosen as the PC substrate if an increase in efficiency is sought. On the other hand, the importance of applying a high bias voltage (the efficiency increases linearly with the bias field $E_b$) also stresses the need for a high-resistivity substrate. A trade-off between these two parameters often arises; even though it is agreed upon that the importance of a high-resistivity device supersedes the mobility requirement. In this regard, LTG-GaAs is well-suited as a substrate material. Annealed LTG-GaAs has a resistivity as high as ~$10^6$ Ω cm (with a break down field of ~5x$10^5$ V/cm) and a reasonably good mobility (100~300 $cm^2$/V/sec) [16, 17].

### 3. Optimization of PC antenna design

Smith, *et al.*[10] reported the study of THz emission spectra observed from PC dipole antennas having three different antenna lengths. They found that the emission intensity significantly decreases as the dipole length, $L$, is decreased from 200 μm to 50 μm. In addition, the dynamics of the transient current induced by the excitation of the PC antenna with a fs laser pulse is another crucial parameter for its THz emission characteristics. The dependence of the emission spectrum on the laser pulse duration was reported by Duvillaret *et al.*[18]. However, the relationship between the geometrical parameters of the antenna design and the temporal characteristics of the transient current has not been well understood. In order to optimize the antenna design for specific applications, this relationship has to be investigated. In this section, we summarize our recent study [19] on the dependence of the THz emission spectrum on the geometrical parameters of the dipole antenna, as well as the correlation between these parameters and the temporal characteristics of the transient current that generates THz radiation.

The dipole PC antennas were fabricated on LTG-GaAs substrates using standard photolithographic techniques. Firstly, we investigated the dependence of the THz radiation characteristics on the dipole length $L$ of the PC antenna. The PC gap, $G$, and the dipole width, $W$, were fixed at 5 μm and 10 μm, respectively. The THz radiation spectra for each of the PC antennas were measured by using standard THz-TDS techniques [20]. THz radiation was generated from PC antennas with various $L$, ranging from 20 to 200 μm and detected by a dipole PC antenna ($L$ = 70 μm and $W$ = 10 μm, and G= 10 μm), optically gated by fs laser pulses (pulse width of $\tau_0$ = 120 fs and wavelength centered at 800 nm). Each PC antenna was fitted with a hemispherical lens to suppress the multiple reflections in the substrate and to enhance the collection efficiency of the THz radiation.

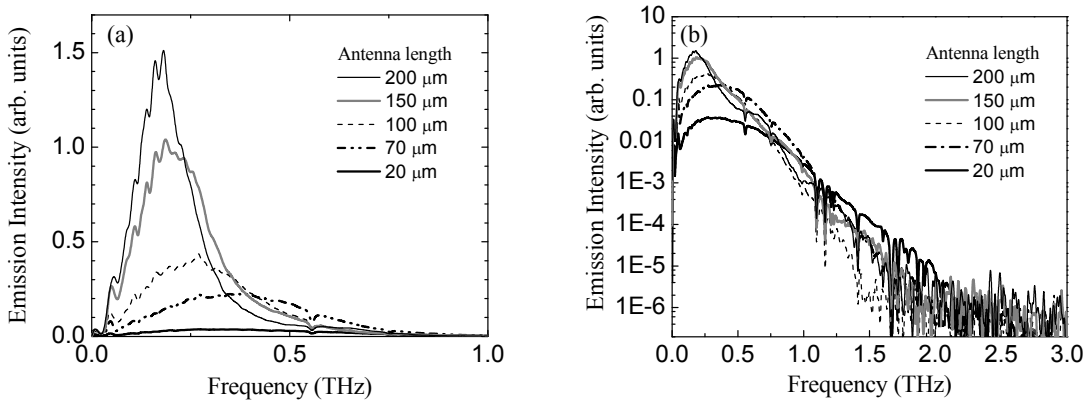


Fig. 2 (a) Power spectra of the THz emission from PC dipole antennas having different antenna lengths ranging from 20 μm to 200 μm. (b) The same spectra in (a) plotted in logarithmic scale, with the frequency range extended to 3 THz.

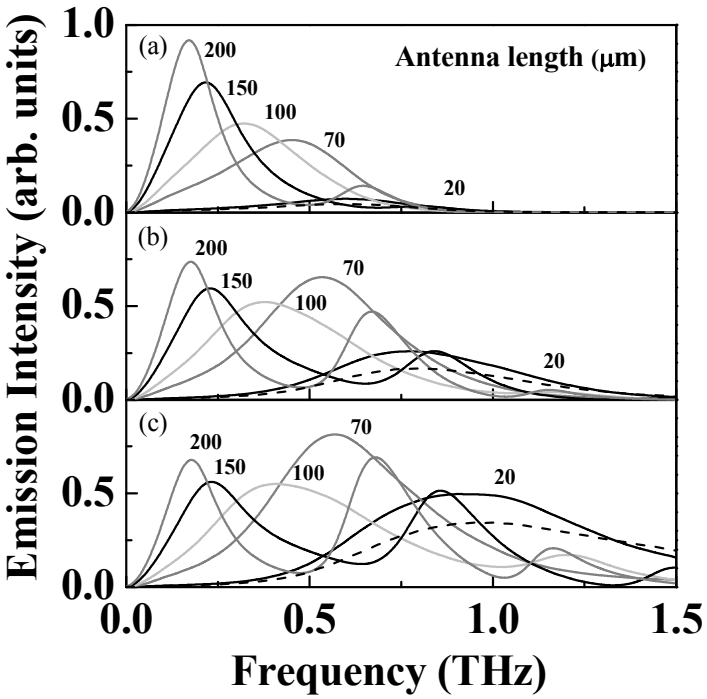


Fig. 3. Calculated emission power spectra for dipole antennas with different dipole lengths ranging from 20 μm to 200 μm for (a) 200 fs , (b) 120 fs, and (c) 80 fs, excitation laser pulses. The emission power spectrum corresponding to the transient input electric field generated by the excitation laser pulse is also shown for reference (dashed black line).

Figure 2(a) shows the measured power spectra of the THz radiation from dipole antennas with different antenna lengths. The highest THz emission intensity was observed for the $L$ = 200 μm antenna (thin solid line). The peak signal decreases consistently as the $L$ value is decreased and the signal for L=20 μm is about 35 times smaller than for $L$ =200 μm. These results agree well with an earlier report [10]. For $L$ = 20 μm (thick solid line), a very broad emission spectrum is observed, with a peak frequency of 0.35 THz. The decrease in emission intensity with decreasing antenna length is accompanied by a gradual bandwidth shift towards higher frequencies. To clearly illustrate this effect, the spectral plots are plotted in logarithmic scale in Fig. 2(b). For frequencies greater than 1 THz, the emission spectrum for $L$ = 20 μm exhibits the highest intensity. These results suggest that the emission frequency bandwidth becomes narrower as the dipole length increases.

In order to explain the experimental results shown in Fig. 2, we calculated the emission spectra using finite-difference time-domain (FDTD) method. To simulate the emission of THz radiation, a transient electric field is applied across the gap of the dipole antenna. The temporal characteristics of this input electric field proportional to $\partial J(t)/\partial t$, is mainly determined by two parameters: the

pulse width of the excitation fs laser pulse, $\tau_0$, and the decay time of the photoexcited carriers, $\tau_c$, in the PC substrate [21]. While keeping a fixed value for $\tau_c$=500 fs, the emission spectra of the transient electric field, $E(t)$, were calculated for three $\tau_0$ values. Figures 3(a), 3(b), and 3(c) show the normalized emission spectra of dipole antennas having different lengths ($L$ = 20, 70, 100, 150, 200 μm) for $\tau_0$ values of 200, 120, 80 fs, respectively. The calculated emission spectrum from the input electric field without the antenna structure is also shown and can be regarded as the reference signal (dashed black curve). The reference data has been magnified for ease of comparison. For $\tau_0$ = 200 fs, Fig. 3(a) shows that the peak intensity increases monotonically and the peak frequency shifts to lower frequency as the antenna length increases. These results are in good agreement with experiment. On the other hand, the emission spectra for shorter $\tau_0$ values in Figs. 3(b) and 3(c), exhibit different antenna length-dependence behavior. The emission spectra for $\tau_0$ = 120 fs in Fig. 3(b) show that the peak intensities for shorter antenna lengths ($L$ = 20, 70 μm) relatively increased; presumably due to the shorter laser pulse width. The red shift of the peak frequency for increasing $L$ values is still apparent. However, shorter laser pulse widths caused the emergence of secondary resonant peaks at 0.71 THz and 0.84 THz for antenna lengths $L$ = 200 μm and 150 μm, respectively. These secondary peaks become more prominent for $\tau_0$ = 80 fs as shown in Fig. 3(c).

The simulation results are explained as follows: When an input electric field has a low-frequency spectrum corresponding to a large $\tau_0$ as in Fig. 3(a), the maximum emission intensity is observed for longer antenna lengths having lower resonance frequencies. This is consistent with the results in Fig.2 even as the actual laser pulse width in the experiment was narrower. The discrepancy in the input electric field pulse width and the actual laser pulse width is attributed to the fact that the simulation did not take into account the antenna detector response. Conversely, input electric fields having higher-frequency spectra should favor antennas with shorter antenna lengths as exemplified in Figs. 3(b) and 3(c). In this latter case, the resonant frequency of the dipole antenna is close to the peak frequency of the input electric field. Moreover, even for longer antenna lengths, large peak intensities can be obtained if the second resonance frequency is close to the peak frequency of the input electric field.

We also investigated the influence of the dipole width, $W$, to the THz emission efficiency and found that the optimization of $W$ is equally important. A thorough discussion is excluded in this text but experiments and simulations indicated that the efficiency of THz radiation decreases with the aspect ratio, $\eta \equiv L/W$, for a constant pump power. Thus, $W$ should be kept narrow for efficient emission of THz radiation.

### 4. 1.55-μm Probe with an LT-GaAs PC antenna

Compact and cost-effective THz-TDS systems necessitate excitation sources of similar attributes. A

fs fiber laser is the best candidate for this requirement. However, LTG-GaAs-based PC antennas have not been used with fiber lasers since LTG-GaAs antennas were believed to be insensitive to wavelengths longer than 870 nm due to the relatively large bandgap of bulk GaAs (1.43 eV at room temperature). Fiber lasers usually emit at 1.55 μm, whose photon energy of 0.8 eV, is much lower than the bandgap of GaAs. Therefore, PC antennas using semiconductors with narrower bandgaps, such as Ge [22] and InGaAs [23-28], have also been investigated. One of the main drawbacks in using narrow bandgap semiconductors, however, is the low resistivity of the PC gap which increases the thermal noise in PC antennas when they are used as THz detectors. Tani, *et al*, [29] reported that a LTG-GaAs PC antenna with 1.55-μm probe has about 10% of the sensitivity of a 780-nm probe at the same power. They attributed the photoconductive response with the 1.55-μm probe to nonlinear absorption associated with deep level defects in LTG-GaAs. Recently, Kataoka, *et al*, [30] reported that the signal level of LTG-GaAs PC antenna can be increased significantly by reducing the PC gap down to 1.5-2 μm and tightly focusing the 1.55-μm probe beam unto the gap. Interestingly, Kataoka *et al* [30] also found that the noise level of the LTG-GaAs PC antenna did not increase with the 1.55-μm probe power, up to a maximum available power of ~13 mW. This indicates that the current noise was lower than the amplifier noise. Their results illustrate that LTG-GaAs is indeed an ideal substrate for PC antennas even with 1.55-μm probe due to its reasonable PC response; along with its high resistivity and short carrier lifetime which suppress the current noise.

Figure 4(a) shows THz time-domain waveforms generated by fs laser optical pumping of a *p*-InAs bulk semiconductor and detected by a 2-μm-gap LTG-GaAs PC antenna using 27 mW, 1.55-μm probe pulses delivered from a fs fiber laser (pulse width ~200 fs, repetition rate ~42 MHz). The pump beam was mechanically chopped at 2 kHz and the average pump power incident on the *p*-InAs was about 60 mW. A magnetic field of ~650 mT parallel to the *p*-InAs surface (and vertical to the reflection plane of the pump beam) was applied to enhance the THz emission from *p*-InAs. The probe beam was focused to the 2-μm PC gap by an aspheric lens. To investigate polarization dependence, the probe beam was polarized parallel (TM-polarization) and perpendicular (TE-polarization) to the dipole direction. Results show that there is a large difference in the detection sensitivity between the TM- and TE-polarized probes. The peak signal for the TM-polarized probe is ~2.7 times higher than the TE-polarization peak signal. Similar polarization dependence of the THz signal was also reported by Huggard, *et al*, [31] for a 5-μm silicon-on-sapphire dipole antenna

probed with 765-nm fs laser pulses. They observed that the TM/TE signal ratios change from 2.6 to 3.3 depending on the probe power (< 6 mW). The low sensitivity for the TE-polarized probe case was attributed to the discontinuities in the lateral intensity distribution near the metal contact.

The power spectra of the two THz waveforms, showing spectral dynamic ranges of more than $10^6$ for both cases, are illustrated in Fig.4(b). The low signal level of the TE probe is compensated by its lower noise-levels and thus the signal-to-noise ratio is comparable to that of the TM-polarized probe case. Figure 5 shows the probe power dependence of the detected peak THz signal for the TM- and TE-polarized probes. The signal increases superlinearly with the probe power due to the nonlinear absorption in LTG-GaAs when the probe power is low, but the signal level of the

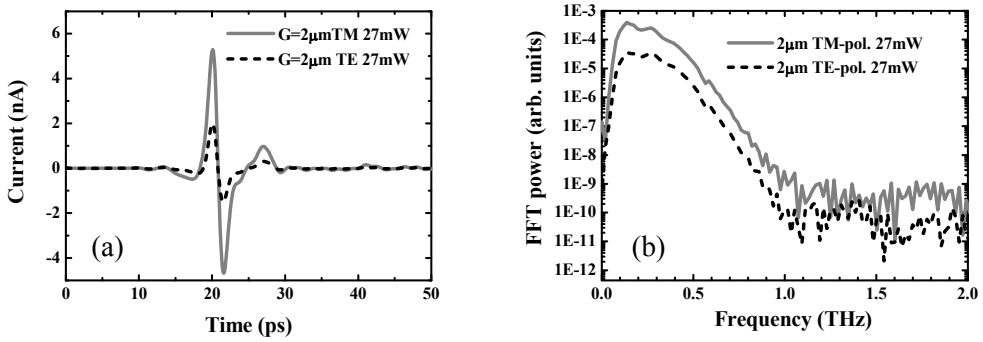


Fig.4. (a) THz time-domain waveforms detected using the 2-μm-gap LTG-GaAs PC antenna with a 1.55-μm fs fiber laser. (b) Corresponding Fourier transform spectra of the time-domain waveforms in Fig. 4(a).

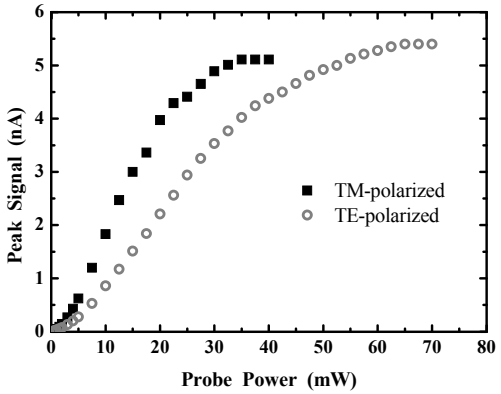


Fig.5. 1.55-μm probe power dependence of the detected peak THz signal using a LTG-GaAs PC antenna for TM-polarization (■) and TE-polarization (○).

saturation condition is the same for both TM- and TE-polarized probe beams. Saturation occurs for probe powers around 30 mW and 60 mW, for TM- and TE-polarization, respectively.

Our results are summarized as follows. (i) Using a narrow PC gap and with tight focusing of the probe beam, we were able to demonstrate sufficient sensitivity for a LTG-GaAs PC antenna detector gated by a 1.55-μm probe beam; (ii) for probe powers below saturation, the PC response is highly sensitive to the probe beam polarization and it was found to be larger for TM-polarization than for TE-polarization; (iii) the PC signal saturation level was inferred to be influenced by the PC antenna gap geometry (length and width), the probe polarization, and focusing optics. Although further parametric studies are needed to fully characterize the PC response of LTG-GaAs antennas for sub-bandgap excitation, results initially suggest that a short-gap (~2-μm) antenna performs as an excellent THz detector when used in conjunction with a tightly focused 1.55-μm TM-polarized probe beam near the saturation power, which is typically 20-30 mW.

**5. Enhanced THz radiation from InSb with lens coupling and magnetic field**

Indium arsenide (InAs) is regarded as one of the best THz emitters among bulk semiconductors at 800 nm laser excitation [32]. On the other hand, indium antimonide (InSb) has been shown to have a stronger emission than InAs with 1.55-μm laser excitation even as its THz emission is much weaker than that of InAs under 800-nm excitation [33-34]. The strong THz emission from these two narrow-bandgap semiconductor materials is attributed to the large difference between their electron and hole mobilities. This difference in mobility creates a transient diffusion current (photo-Dember current) at the surface-normal upon fs laser excitation. Aside from their simplicity and robustness, one of the advantages of these semiconductors as THz emitters is their compatibility with 1.55-μm laser sources. InAs has exhibited significant THz emission enhancement by an applied magnetic field, [35] as well as by using a surface coupling prism or lens [36-38]. On the other hand, InSb has been not been thoroughly investigated for similar enhancement studies. As such, further investigation on the THz emission from InSb for 1.55-μm excitation and its emission enhancement properties using various methods is crucial for investigating its feasibility as a THz emitter. In this section, we describe the enhancement of THz emission from bulk InSb by using a surface coupling substrate lens and an applied magnetic field for 1.55-μm fs laser excitation.

A fs fiber laser with a dual-wavelength output (47.5-MHz repetition rate, <300fs for 1.55-μm fundamental output and 100-fs for 780 nm SHG output) was used to irradiate a *p*-InSb (carrier density $n$= 2-3 x $10^{15}$ $cm^{-3}$ and electron mobility $\mu$ = 8.4-4.9 x $10^{3}$ $cm^{2}$/V/sec at 77K) single crystal

and to optically gate (probe) a PC antenna detector. The thickness of the wafer was ~0.45 mm. A ~650 mT magnetic field in the "upward" direction was applied to the sample. In addition, a Si hemispherical substrate lens with a diameter of 3 mm was placed at the irradiated surface of the sample. The fundamental 1.55-μm pump beam was separated from the second harmonic 780-nm probe beam by a polarizing beam splitter. The average pump and probe beam powers were 12 mW and 20 mW, respectively. The pump beam was mechanically chopped at 2-kHz and focused to the *p*-InSb surface with an incident angle of $45^{O}$. The focal spot size of the pump beam on the sample was estimated from the beam diameter and the focal length of the focusing lens to be ~350 μm. The emitted THz wave was collimated and redirected towards the LTG-GaAs dipole PC antenna THz detector by a pair of off-axis parabolic mirrors.

The THz time-domain waveforms from *p*-InSb with and without the lens coupler and magnetic

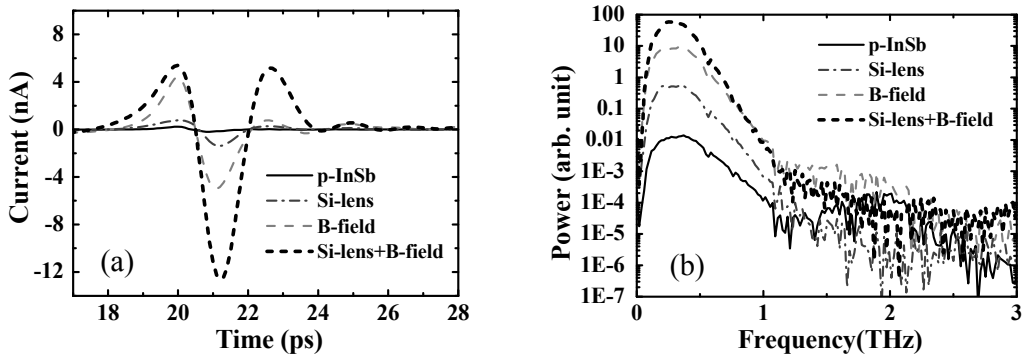


Fig. 6. (a) THz time-domain waveforms from *p*-type InSb with and without a Si lens and magnetic field. (b). Fourier transformed spectra of the THz time-domain waveforms in Fig. 6 (a).

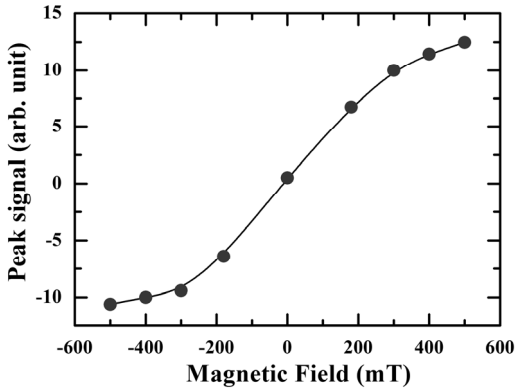


Fig 7. The magnetic field dependence of the peak signal of the THz time-domain waveform emitted from *n*-type InSb.

field are shown in Fig. 6(a). An enhancement of around 24 times in THz emission amplitude was achieved with a magnetic field of ~650 mT. In addition, an enhancement of around 7 times in THz emission amplitude was achieved with the attachment of a Si lens. Furthermore, a total of around 60 times in THz emission amplitude was realized by combining the Si hemispherical lens and magnetic field.

The magnetic field enhancement can be explained by the Lorentz force exerted on to the excited carriers in the semiconductor [35]. This force changes the direction of the photo-Dember current away from the surface normal; thereby rotating the dipole emission pattern towards the surface and improves the THz emission efficiency from the surface to free space. Aside from its focusing properties, the Si hemispherical lens reduces the total reflection loss of the THz radiation at the interface of the semiconductor and outer media by acting as an index-matching material. The THz emission outside the cone, limited by the critical angle $\alpha_C$ (with its axis normal to the semiconductor surface), is totally reflected. The critical angle $\alpha_C$ is $14.1^O$ for bare InSb ($n_{InSb} = 4.1$) while it is increased to $58.5^0$ by using the Si lens ($n_{Si} = 3.41$). Thus, the radiation loss due to total internal reflection can be significantly reduced by using a substrate lens with a high refractive index such as Si ($n_{Si} = 3.41$).

Figure 6(b) shows the Fourier-transformed power spectra of the THz time-domain waveforms. The THz signal level was comparable to that of a typical PC antenna and a dynamic range of more than $10^6$ was achieved with the simultaneous enhancement of the magnetic field and the Si lens. The emission spectrum of the InSb with the lens coupler is slightly shifted to lower frequencies. This can be explained by the effect of the coupling lens leading to a more efficient collection of the lower-frequency components, otherwise lost by diffraction. A similar frequency shift has been reported for THz emission from InAs with a MgO lens in a reflection geometry setup [37] and also for THz emission from InAs thin films with a Si lens in transmission geometry [38].

Figure 7 shows the magnetic field dependence of the peak signal of the THz-TDS waveform emitted from *n*-type InSb without a coupling lens (note that the THz emission efficiency and the magnetic field dependence with *n*-type InSb are similar to those of *p*-type InSb). The magnetic field enhancement is almost saturated at ~500 mT, indicating that at this value, the dipole emission pattern has already been reoriented almost in the same direction as the surface-normal of the semiconductor.

## 6. Summary

In summary, we have investigated techniques and design principles for improving THz-TDS systems. Our investigation included the following: (i) the influence of the design parameters, *L* and *W*, of dipole-type PC antennas to their THz emission spectra, (ii) the dependence of the THz detection

sensitivity and saturation properties of a 2 μm-gap PC antenna on the 1.55-μm probe polarization, and (iii) enhanced THz emission from *p*-InSb by the combined effects of a coupling substrate lens and a magnetic field. The findings and techniques reported here provide valuable information on the design of an efficient, compact and cost-effective THz-TDS system, based on 1.55-μm fs laser sources.

**Acknowledgements**

This work was supported in part by a grant program from the Development of Systems and Technology for Advanced Measurement and Analysis, Japan Science and Technology Agency (JST), and also by a grant program from the Feasibility Study Stage in Adaptable and Seamless Technology transfer Program (FS-stage, A-STEP), JST.

**References**

[1] S. Jayaraman and C. H. Lee, Appl. Phys. Lett. 20, 392 (1972)

[2] C. H. Lee, Appl. Phys. Lett. 30, 84 (1977)

[3] D. H. Auston, Appl. Phys. Lett. 26, 101 (1975)

[4] D. H. Auston, K. P. Cheung, and P. R. Smith, Appl. Phys. Lett. 45, 284 (1984)

[5] G. Mourou, C. V. Stancampiano, A. Antonetti, and A. Orszag, Appl. Phys. Lett. 39, 295 (1981)

[6] M. Hangyo, M. Tani and T. Nagashima, Int. J. Infrared Millli. Waves 26, 1661 (2005)

[7] J. A. Zeitler, Y. C. Shen, C. Baker, P. F. Taday, M. Pepper, and T. Rades, J. Pharm. Sci. 96, 330 (2007)

[8] L. Ho, R. Müller, M. Römer, K.C. Gordon, J. Heinämäki, P. Kleinebudde, M. Pepper, T. Rades, Y. C. Shen , C. J. Strachan, P. F. Taday, and J. A. Zeitler, J. Control. Rel. 119, 253 (2007)

[9] K. Fukunaga, Y. Ogawa, S. Hayashi, and I. Hosako, IEICE Electron. Exp. 4, 258 (2007)

[10] P. R. Smith, D. H. Auston, and M. C. Nuss, IEEE J. Quantum Electron. 24, 255 (1988)

[11] Martin van Exter, Ch. Fattinger, and D. Grischkowsky, Appl. Phys. Lett. 55, 337 (1989)

[12] Martin van Exter and D. Grischkowsky, IEEE Trans. Micro. Theory Tech., 38, 1684, (1990)

[13] N. Katzenellenbogen and D. Grischkowsky, Appl. Phys. Lett. 58, 222 (1991)

[14] A. C. Warren, N. Katzenellenbogen, D. Grischkowsky, J. M. Woodall, M. R. Melloch, and N. Otsuka, Appl. Phys. Lett. 58, 1512 (1991)

[15] D. Grischkowsky, S. Keidng, Martin van Exter, and Ch. Fattinger, J. Opt. Soc. Am. B 7, 2006 (1990)

[16] S. Gupta, J. F. Whitaker, and G. A. Mourou, IEEE J. Quantum Electron. 28, 2464 (1992)

[17] D. C. Look, Thin Solid Films 231, 61 (1993)

[18] L. Duvillaret, F. Garet, J.-F. Roux, and J.-L. Coutaz, IEEE J. Select. Topics Quant. Elect. 7, 615 (2001)

[19] F. Miyamaru, Yu Saito, K. Yamamoto, T. Furuya, S. Nishizawa, and M. Tani, Appl. Phys. Lett. 96, 211104 (2010)

[20] M. Hangyo, T. Nagashima, and S. Nashima, Meas. Sci. Technol. 13, 1727 (2002)

[21] S. Hughes, M. Tani, and K. Sakai, J. Appl. Phys. 93, 4880 (2003)

[22] N. Sekine, K. Hirakawa, F. Sogawa, Y. Arakawa, N. Usami, Y. Shiraki, and T. Katoda, Appl. Phys. Lett. 68, 3419 (1996)

[23] M. Suzuki and M. Tonouchi, Appl. Phys. Lett. 86, 163504 (2005)

[24] M. Suzuki and M. Tonouchi, Appl. Phys. Lett. 86, 051104 (2005)

[25] N. Chimot, J. Mangeney, L. Joulaud, P. Crozat, H. Bernas, K. Blary, and J. F. Lampin, Appl. Phys. Lett. 87, 193510 (2005)

[26] A. Takazato, M. Kamakura, T. Matsui, J. Kitagawa, and Y. Kadoya, Appl. Phys. Lett. 90, 101119 (2007)

[27] A. Takazato, M. Kamakura, T. Matsui, J. Kitagawa, and Y. Kadoya, Appl. Phys. Lett. 91, 011102 (2007)

[28] M. Sukhotin, E. R. Brown, A. C. Gossard, D. Driscoll, M. Hanson, P. Maker, and R. Muller, Appl. Phys. Lett. 82, 3116 (2003)

[29] M. Tani, K-S Lee, and X.-C. Zhang, Appl. Phys. Lett. 77, 1396 (2000)

[30] T. Kataoka, K. Kajikawa, J. Kitagawa, Y. Kadoya, and Y. Takemura, Appl. Phys. Lett. 97, 201110 (2010)

[31] P. G. Huggard, C. J. Shaw, J. A. Cluff, and S. R. Andrews: Appl. Phys. Lett. 72, 27 (1998)

[32] G. Chern, E. Readinger, H. Shen, M. Wraback, C. Gallinat, G. Koblmüller, and J. Speck, Appl. Phys. Lett. 89, 141115 (2006)

[33] R. Adomavičius, G. Molis, A. Krotkus, and V. Sirutkaitis, Appl. Phys. Lett. 87, 261101 (2005)

[34] M. Suzuki, M. Tonouchi, K. Fujii, H. Ohtake, and T. Hirosumi, Appl. Phys. Lett. 89, 091111 (2006)

[35] N. Sarukura, H. Ohtake, S. Izumida, and Z. Liu, J. Appl. Phys. 84, 654 (1998)

[36] M. B. Johnston, D. M. Whittaker, A. Dowd, A. G. Davies, E. H. Linfield, X. Li, and D. A. Ritchie, Opt. Lett. 27, 1935 (2002)

[37] M. Nakajima, K. Uchida, M. Tani, and M. Hangyo, Appl. Phys. Lett. 85, 191 (2004)

[38] C. T. Que, T. Edamura, M. Nakajima, M. Tani, and M. Hangyo, Jpn. J. Appl. Phys. 50, 080207 (2011)